Journal of Solid State Chemistry 182 (2009) 2997–3002

Contents lists available at ScienceDirect

Journal of Solid State Chemistry

journal homepage: www.elsevier.com/locate/jssc

Swelling, intercalation, and exfoliation behavior of layered ruthenate derived from layered potassium ruthenate

Katsutoshi Fukuda [a], Hisato Kato [b], Jun Sato [b], Wataru Sugimoto [a,b,*], Yoshio Takasu [b]

[a] Collaborative Innovation Center for Nanotech Fiber, Shinshu University, 3-15-1 Tokida, Ueda, Nagano 386-8567, Japan
[b] Faculty of Textile Science and Technology, Shinshu University, 3-15-1 Tokida, Ueda, Nagano 386-8567, Japan

ARTICLE INFO

Article history:
Received 14 May 2009
Received in revised form
3 August 2009
Accepted 10 August 2009
Available online 15 August 2009

Keywords:
Layered ruthenium oxide
Swelling
Intercalation
Exfoliation
Nanosheet

ABSTRACT

The intercalation chemistry of a layered protonic ruthenate, $H_{0.2}RuO_{2.1} \cdot nH_2O$, derived from a layered potassium ruthenate was studied in detail. Three phases with different hydration states were isolated, $H_{0.2}RuO_{2.1} \cdot nH_2O$ ($n = \sim 0$, 0.5, 0.9), and its reactivity with tetrabutylammonium ions (TBA^+) was considered. The layered protonic ruthenate mono-hydrate readily reacted with TBA^+, affording direct intercalation of bulky tetrabutylammonium ions into the interlayer gallery. Fine-tuning the reaction conditions allowed exfoliation of the layered ruthenate into elementary nanosheets and thereby a simplified one-step exfoliation was achieved. Microscopic observation by atomic force microscopy and transmission electron microscopy clearly showed the formation of unilamellar sheets with very high two-dimensional anisotropy, a thickness of only 1.3 ± 0.1 nm. The nanosheets were characterized by two-dimensional crystallites with the oblique cell of $a = 0.5610(8)$ nm, $b = 0.5121(6)$ nm and $\gamma = 109.4(2)^\circ$ on the basis of in-plane diffraction analysis.

1. Introduction

Unilamellar two-dimensional crystallites, so-called "exfoliated nanosheets", obtained by total delamination of various layered oxides with ion-exchange capabilities [1–11] have attracted significant attention as a unique class of nano-scale materials in solid state chemistry. These nanosheet crystallites have thickness in the range of molecular scale and lateral size in bulk dimension. Such high structural anisotropy is quite different from that of other nanomaterials, which are usually spherical or rod-like in shape. They often exhibit intriguing physicochemical properties that cannot be attained by bulk materials due to its unique two-dimensionality [12–14]. Furthermore, the intrinsically negative-charged nanosheets can be easily re-assembled into three-dimensional architectures by various methods. The parent layered material can be synthesized with a vast range of compositions via typical ceramic routes, allowing nanosheets with a comprehensive composition range as long as total exfoliation can be accomplished. In particular, metal oxide nanosheets with functionalities inherited from their parent materials are important inorganic building blocks for the fabrication of a variety of well-ordered nanostructured materials [15–17], through which rational design and control of functionalities can be achieved.

Rutile-type RuO_2 has a number of attractive properties atypical of most oxide systems, including metallic conductivity [18], electrocatalytic activity [19] and excellent chemical and electrochemical stability [20]. Ruthenate nanosheets [21] obtained via delamination of layered potassium ruthenate can be regarded as a new family of the versatile ruthenium dioxide. We have studied these ruthenate nanosheets in terms of their electrochemical properties for electrochemical energy storage and conversion applications [21–23]. The interlayer nano-space of the layered ruthenate can be utilized for electrochemical charge storage, leading to an extremely large pseudocapacitance of $\sim 400\,F\,g^{-1}$ despite the micro-sized particles. In addition, total exfoliation leads to a significant enhancement in pseudocapacitance reaching capacitance of $660\,F\,g^{-1}$ for the materials in which the ruthenate nanosheets were re-stacked via a simple casting–drying technique [21]. The ruthenate nanosheets also act as an effective and durable co-catalyst for electro-oxidation of carbon monoxide and methanol, finding use as electrocatalysts in fuel cells [23]. The conductive ruthenate nanosheets are thus promising materials for current and emerging applications in energy-related applications. Yet, many principles of this oxide system, in particular the intercalation chemistry of the layered precursor and molecular entity of the obtained nanosheets, are still not well understood.

In our previous work [21], the ruthenate nanosheets were derived through a successive series of chemical processes; (i) ion-exchange of the interlayer potassium ions to protons through acid treatment, (ii) incorporation of *n*-alkylamine via acid–base reaction to expand the interlayer gallery and (iii) guest exchange

* Corresponding author at: Faculty of Textile Science and Technology, Shinshu University, 3-15-1 Tokida, Ueda, Nagano 386-8567, Japan. Fax: +81 268 21 5452.
E-mail address: wsugi@shinshu-u.ac.jp (W. Sugimoto).

0022-4596/$ - see front matter © 2009 Elsevier Inc. All rights reserved.
doi:10.1016/j.jssc.2009.08.012

of the interlayer alkylammonium ions with bulky tetrabutylammonium ions (TBA^+) which is used as the exfoliation reagent. The resulting TBA^+/ruthenate intercalation compound could be exfoliated into elemental nanosheets, by suspending the powder in water or organic solvents with high dielectric constant. However, this multi-step route makes the formation process of the nanosheets very complicated, resulting inevitably in a low yield.

In addition, the previous study focused on the intercalation chemistry of the anhydrous system obtained via heating of the as-prepared wet samples at 120 °C so as to carefully characterize the proton-exchanged forms [21]. Owing to the relatively smaller interlayer distance of the dried products, the dehydrated layered ruthenate did not react readily with the bulky TBA^+. Therefore, the intricate process involving the acid–base reaction using the smaller ammonium ions to enlarge the interlayer in advance was adopted. In this work, we anticipated that hydration accompanying the proton-exchange process might also afford an expanded interlayer gallery similar to the intermediate *n*-alkylammonium intercalation compound, which in turn may promote the incorporation of TBA^+ into the interlayer gallery by a more straightforward process.

This present paper deals with the hydration, dehydration, and re-hydration behavior of layered protonic ruthenate. The swelling and delamination behaviors of the layered potassium ruthenate were studied systematically in detail. Particular attention was paid to explore a more simplified, direct and facile route to total exfoliation by the direct reaction of TBA^+ with the hydrated phase. Unique structural features of the exfoliated ruthenate nanosheets in unilamellar state were also characterized.

2. Experimental section

Layered potassium ruthenate was synthesized as a starting material by heating a pelletized mixture of K_2CO_3 and RuO_2 (5:8 molar ratio) at 850 °C for 12 h under Ar atmosphere [21]. The product was washed with ultra-pure water (>18 MΩ cm) to remove water-soluble minor components. The isolated potassium ruthenate (formulated as $K_{0.2}RuO_{2.1}\cdot nH_2O$) [21,22] was treated with aqueous 1 mol dm^{-3} HCl for 3 days or 0.5 mol dm^{-3} H_2SO_4 for 2 days at 60 °C to promote complete proton exchange. The acid solutions were replaced everyday. The acid-treated ruthenate, $H_{0.2}RuO_{2.1}\cdot 0.9H_2O$, (0.1 g) was added to 25 cm^3 of aqueous TBAOH with various concentrations and shaken vigorously for at least 10 days. The concentration of TBAOH was controlled so that the TBA^+ to H^+ ratio, where H^+ is the ion-exchangeable proton content in the layered protonic ruthenate, was varied between $TBA^+/H^+ = 0.1$ and 30 to optimize the exfoliation degree. The resultant auburn suspensions were first centrifugated at 2000 rpm for 30 min to separate the exfoliated nanosheets and the readily sedimenting material. For estimation of the exfoliation yield, the supernatant was dried and heated to 550 °C in air to convert the protonic ruthenate to rutile-type RuO_2.

Layer-by-layer assembly of ruthenate nanosheets onto a silicon substrate was conducted as follows. Si wafer was cleaned by dipping in 12 mol dm^{-3} aqueous HCl+24 mol dm^{-3} aqueous CH_3OH (1:1 by volume) solution and then in 18 mol dm^{-3} aqueous H_2SO_4 solution to obtain a hydrophilic surface. The substrate was immersed in an aqueous solution containing poly-diallyldimethylammonium chloride (pH = 9, 2.5 g dm^{-3}), a polycation commonly used as a counter-part in the layer-by-layer self-assembly, [15,16] for 10 min. Then, it was dipped in a colloidal suspension of negatively charged nanosheets (pH = 10.2, 0.08 g dm^{-3}) for 60 min to assemble a monolayer film, in which the nanosheets were adsorbed in random azimuth via electrostatic self-assembly onto the substrate surface.

Powder X-ray diffraction (XRD) data were collected by means of Bragg-Brentano-type diffractometers (Rigaku Rint 2000) with Cu*K*α radiation ($\lambda = 0.15405$ nm). Mass loss up to 500 °C was measured by thermogravimetry (Rigaku Thermo Plus TG 8120). Optical absorption spectra for the diluted nanosheet suspensions in a quartz cell were recorded on a Hitachi U-4100 spectrophotometer. A tapping-mode atomic force microscope (AFM; Seiko Instruments SPA400) with Si-tip cantilever (20 N m^{-1}) was used to characterize morphological features of the nanosheets on a flat substrate. Transmission electron microscopy (TEM) was performed with a JEOL 2010 operated at an accelerating voltage of 200 kV. Specimens for these observations were prepared by directly placing droplets of the nanosheet suspension diluted with pure water onto a hydrophilic Si substrate and a holey collodion supported Cu grid, respectively. In-plane diffraction pattern of the self-assembled film of the nanosheets was measured by a four-axis diffractometer equipped with NaI scintillation counter at the BL-6C of the Photon Factory in the High Energy Accelerator Research Organization.

3. Results and discussion

3.1. Intercalation chemistry of hydrous layered ruthenates

The XRD pattern of the starting parent material (layered potassium ruthenate, average composition $K_{0.2}RuO_{2.1}\cdot 0.5H_2O$) exhibited a series of sharp diffraction peaks at 12.04°, 24.25° and 36.75° ($d = 0.734$, 0.367 and 0.244 nm, respectively) as shown in Fig. 1. These peaks are assignable to the reflections arising from basal planes of the ruthenate host layer. The acid-treated product without any drying process shows a clear shift of the reflection peaks to lower diffraction angle compared to the parent $K_{0.2}RuO_{2.1}\cdot 0.5H_2O$ (Fig. 1b), indicating an expansion of the basal spacing from 0.734 to 0.785 nm. The as-prepared acid-treated product has an average chemical composition of $H_{0.2}RuO_{2.1}\cdot 0.9H_2O$ based on the mass loss upon heating. This product gradually undergoes dehydration into an intermediate phase, $H_{0.2}RuO_{2.1}\cdot 0.5H_2O$, when left standing for prolonged duration under ambient condition. Despite the lower hydration state, the lowest angle diffraction peak shifted to lower angle with a larger spacing of 1.249 nm (Fig. 1c). Complete dehydration to the

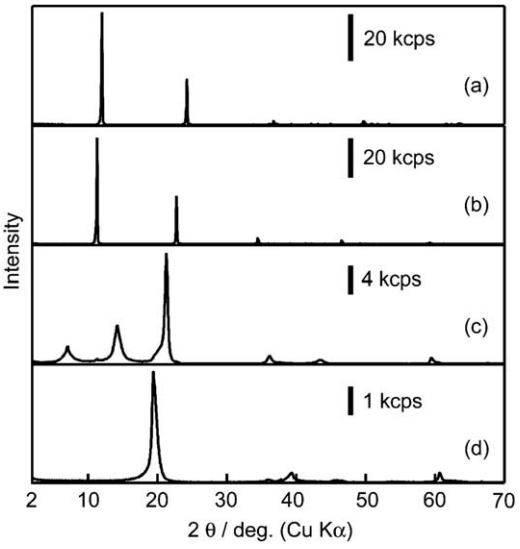

Fig. 1. XRD patterns for (a) hydrated layered potassium ruthenate, (b) as-prepared hydrated protonic form, (c) partially dehydrated form and (d) completely dehydrated form.

anhydrous phase can be accomplished by heating at 180 °C. The anhydrous layered protonic ruthenate phase has a smaller interlayer gallery of 0.456 nm (Fig. 1d). It should be noted that the intensity distribution of the basal reflections observed in the intermediate phase, $H_{0.2}RuO_{2.1}\cdot 0.5H_2O$, are quite different compared to those of the other mono-hydrate and anhydrous phases. This behavior may be explained by staging. In fact, the sum of 0.785 nm spacing for the mono-hydrate and 0.456 nm spacing for the anhydrate yields a spacing of 1.241 nm, which is consistent with the observed diffraction series of 1.249 nm spacing for the intermediate phase. Such staging behavior is rather uncommon for layered transition metal oxides, but can be induced by hydration or dehydration in some clay minerals [24]. Interestingly, the intermediate and anhydrous phases do not re-hydrate (see Fig. S1). As a consequence, the intermediate and anhydrous phases have poor ion-exchange property with foreign species and bulky TBA^+ cannot enter the interlayer gallery of these two phases. Stronger interaction such as acid–base type reaction with *n*-alkylamines must be used to expand the interlayer of the dried products. However, the mono-hydrated phase can react with bulky TBA^+ as will be discussed below. Therefore, the protonic ruthenate mono-hydrate, having the largest interlayer distance, was used as the precursor for further investigation of the preparation of exfoliated ruthenate nanosheets.

3.2. Exfoliation of layered protonic ruthenate mono-hydrate into dispersed nanosheets

The obtained layered protonic ruthenate mono-hydrate was added to aqueous TBAOH solutions with different TBA^+/H^+ ratios and vigorously shaken for 10 days. Auburn suspensions were obtained as displayed in the digital photographs in Fig. 2a. When the suspensions were left standing for 10 days after vigorous shaking, a clear difference in the sedimentation behavior was noticeable with the bare eye. At $TBA^+/H^+ \leq 1$, powdery deposits on the bottom of the reaction vessel were observed, and the supernatant became clear. At $TBA^+/H^+ > 1$, very stable colloidal suspensions were formed. A slight but noticeable amount of precipitate is observed when the shaken solution is left standing for a prolonged period of time. The amount of precipitate seems smallest when $TBA^+/H^+ = 5$. The precipitate could be easily separated from the stable colloidal suspension by centrifugation at 2000 rpm for 30 min. Even after the centrifugal separation, a considerable amount of colloid is present, as can be observed by the color of the supernatant.

Fig. 3a shows the XRD pattern of the precipitate collected for the sample with $TBA^+/H^+ = 1$. The XRD pattern suggests the

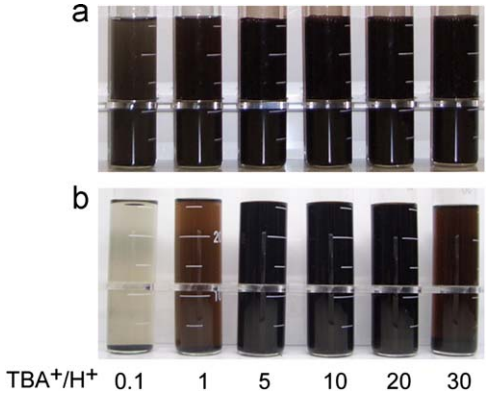

Fig. 2. Photographs of the layered protonic ruthenate reacted with aqueous TBAOH at different TBA^+/H^+ ratios: (a) after vigorous shaking and (b) 10 days left standing after vigorous shaking.

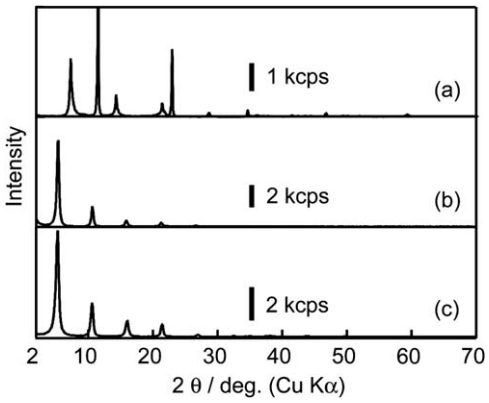

Fig. 3. XRD patterns for (a) spontaneous sediment at $TBA^+/H^+ = 1$, (b) thin film obtained by drying the nanosheet suspension of $TBA^+/H^+ = 10$, and (c) spontaneous sediment at $TBA^+/H^+ = 30$.

presence of two phases with different basal spacing of $d = 0.779$ and 1.247 nm ($2\theta = 11.36°$ and 7.08°, respectively). The former phase is attributed to the un-reacted protonic ruthenate mono-hydrate. The latter phase with a basal spacing of $d = 1.247$ nm matches neither that of the staging compound, in particular, with respect to the intensity distribution nor the TBA^+-ruthenate intercalation compound ($d = 1.68$ nm) obtained by the multi-step process in our previous study [21]. A possible explanation for this basal spacing, $d = 1.247$ nm, may be that the intersheet separation in this phase stem from the simple accommodation of TBA^+ with an estimated size of more or less 0.9 nm [25,26]; the $d = 0.456$ nm spacing of the anhydrous layered protonic ruthenate is composed of the size of an intercalated proton and sheet thickness of ruthenium oxide layer, implying that the host layer is identified as a nearly coplanar array of edge-shared $Ru^{4+}O_6$ octahedra. This very thin host system is believed to give the $d = 1.247$ nm phase in case TBA^+ are accommodated as a monolayer in the gallery as observed in the TBA intercalation process to the α-$NaFeO_2$-type protonic layered manganese oxide system [26]. The $d = 1.68$ nm phase observed in our previous work could be accounted for by the insertion of additional water molecules.

A thin film obtained by casting the nanosheet colloid obtained with $TBA^+/H^+ = 10$ on a Si wafer after drying exhibited only a series of harmonic reflections, $d = 1.682$, 0.829 and 0.561 nm, (Fig. 3b). These peaks are consistent with that of the XRD pattern of re-stacked ruthenate nanosheets, which is an oriented film of a TBA^+-ruthenate intercalation compound [21]. This fact strongly implies that the colloidal suspension obtained in this work by a one-step process contains elementarily exfoliated ruthenate nanosheets. The amount of the colloidal species apparently decreases at the TBA^+/H^+ ratio higher than 20, as can be seen in Fig. 2b. The dark-brown precipitate formed as a major component at $TBA^+/H^+ = 30$ exhibited an XRD pattern similar to that of the re-stacked nanosheets (see Fig. 3c), indicating that intense interlayer separation occurred at this ratio due to the insertion of TBA ions and water molecules. Clearly, the precipitates obtained at $TBA^+/H^+ = 1$ and 30 are different in terms of the reaction with TBAOH aqueous solution. Irrespective of the TBA^+/H^+ ratio, it is clear that TBA^+ was incorporated into the interlayer gallery of the layered ruthenate as long as the mono-hydrate is used as the starting material.

The results obtained in this study revealed that there is a large difference in the swelling behavior depending on the TBA^+/H^+ ratio. This behavior may be in accordance with other nanosheet systems [26,27]. Sasaki and co-workers have investigated the swelling behavior of several layered oxides upon reaction with

TBA^+ in detail and showed that intercalation reaction occurs at low TBA^+/H^+ ratio and changes to osmotic swelling behavior at the higher ratios with exfoliation at the intermediate range.

Optical absorption spectra of the suspension obtained at $TBA^+/H^+ = 10$ were acquired to investigate the degree of exfoliation. The colloidal ruthenate exhibited two broad peaks at wavelengths 360 and 500 nm and an intense absorbance increase below wavelength of 250 nm as displayed in Fig. 4. The absorbance at 360 nm was proportional to the concentration (Fig. 4 inset). This linear relationship implies that the parent layered protonic ruthenate delaminated in mono-dispersed fragments, i.e. exfoliated nanosheets. The molar extinction coefficient for the dispersed nanosheets with chemical composition of $RuO_{2.1}^{0.2-}$ was estimated to be 7.4×10^3 and $5.5 \times 10^3\,mol^{-1}\,dm^3\,cm^{-1}$ at 360 and 500 nm, respectively.

The yield of the dispersed nanosheets in the colloidal suspension after centrifugal separation of the precipitate was evaluated. The colloidal suspension was dried and heated at 550 °C, which results in complete burn-off of water and organic compounds. The yield was calculated by measuring the mass of the solid after heat-treatment. The nanosheet yield is plotted against the TBA^+/H^+ ratio in Fig. 5. A volcano-type plot is obtained with the highest yield of ~70% at $TBA^+/H^+ = 3$. Higher ratios were less favorable in terms of the formation of the dispersed nanosheet.

Our previous multi-step method that used the TBA^+-ruthenate intercalation compound as a starting material of the exfoliated nanosheets may be classified as $TBA^+/H^+ \leq 1$ in this study. Although quantitative comparison of the yield between them is somewhat difficult because of the different ratio of solid to solution, optimizing the TBA^+/H^+ ratio in the more simplified method certainly brings about improvement of the yield and purity, which promises to accelerate further fundamental studies and applications using this material.

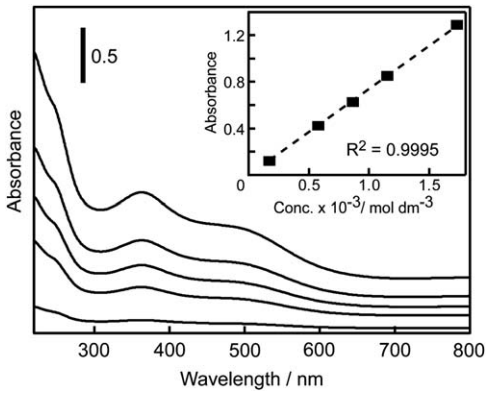

Fig. 4. UV–vis absorption spectra obtained from the colloidal suspension of the ruthenate nanosheets with various concentrations. Inset shows a plot of the absorbance at 360 nm against the concentration of diluted suspension.

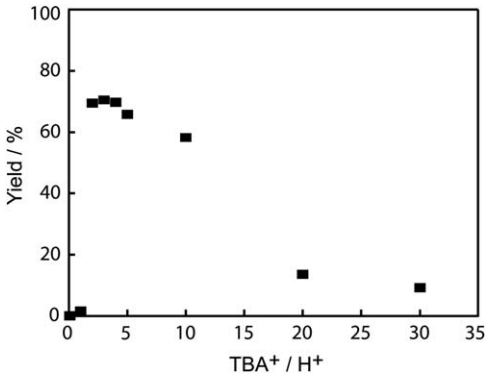

Fig. 5. A plot of the yield of the nanosheet suspension against the TBA^+/H^+ ratio.

3.3. Characterization of ruthenate nanosheet in the unilamellar state

Understanding the molecular entity of the exfoliated nanosheets is of importance for various applications, which is usually attained through characterizations of the nanosheet in unilamellar state [28–30]. A typical AFM image displayed in Fig. 6 of the nanosheets deposited on a cleaned Si substrate revealed a number of islands with uniform height and a lateral size ranging from several hundred nanometers to about 1 μm. The average apparent thickness was calculated as 1.3 ± 0.1 nm by measuring the height difference between the island and the substrate surface. Judging from the observed apparent thickness, the crystallographic thickness of the ruthenate nanosheet is believed to be as thin as other oxide nanosheet systems, approximately 0.4–0.5 nm. For example, in the case of the titanate nanosheets with crystallographic thickness of ~0.4 nm [28], average thickness of about 1.2–1.3 nm was measured by the same AFM technique. This apparent larger thickness observed by the AFM technique was explained by the presence of adsorbed species, possibly water molecules and charge compensating protons, on the surface of the anionic nanosheet [28]. The accurate crystallographic thickness of the ruthenate nanosheets cannot be defined at present, as the precise crystal structure of the parent layered potassium ruthenate has still not been solved. However, combined with the *d*-spacing of 0.456 nm observed by XRD for the anhydrous layered protonic ruthenate, the observed thickness of the ruthenate nanosheets by AFM is strong evidence of complete elemental exfoliation of the parent material. TEM observation also provided information on the morphological feature of the ruthenate nanosheet. A typical TEM image shown in Fig. 7 depicts a two-dimensional sheet with weak but uniform contrast and lateral dimension of sub-micrometer scale similar to those observed in the AFM image. This observation also supports the formation of unilamellar ruthenate nanosheets in the suspension.

Fig. 8 shows a synchrotron radiation in-plane XRD pattern for the self-assembled monolayer film in which the ruthenate nanosheets lay parallel to the substrate surface (its morphological visualization by AFM is appended as Fig. S2). The ruthenate nanosheet monolayer film exhibited many sharp in-plane diffractions in the $1/d$ region from 2.2 to 8.2 nm^{-1}. All of the observed peaks are indexed to *h k* reflections of a two-dimensional oblique cell. The indexes and *d* values are summarized in Table 1. The refined cell parameters were $a = 0.5610(8)$ nm, $b = 0.5121(6)$ nm and $\gamma = 109.4(2)^\circ$. Clearly, the exfoliated

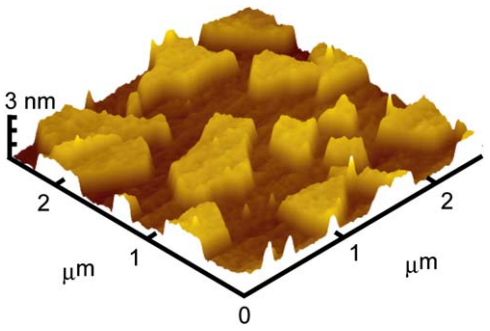

Fig. 6. A typical AFM image of the ruthenate nanosheets deposited on a Si substrate in isometric projection.

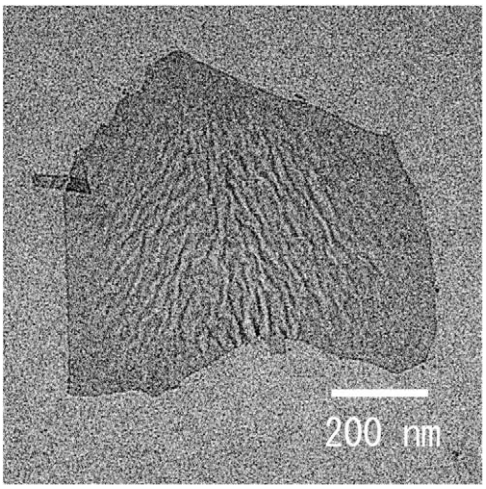

Fig. 7. A typical TEM image of a ruthenate nanosheet deposited on a holey collodion supported Cu grid.

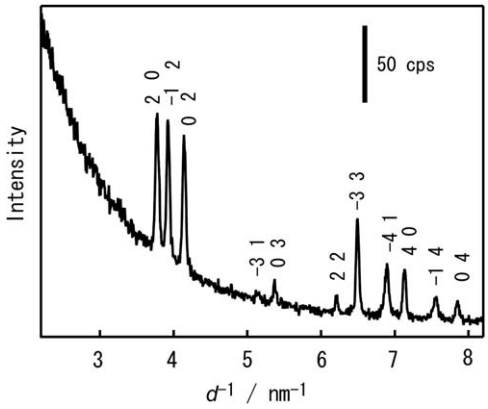

Fig. 8. An in-plane XRD diffraction pattern for the monolayer film of the ruthenate nanosheets.

Table 1
Indexes and *d* values of observable in-plane diffractions.

hk	*d* (nm)
20	0.2648
−12	0.2547
02	0.2414
−31	0.1862
03	0.1610
22	0.1540
−33	0.1451
−41	0.1402
40	0.1324
−14	0.1274
04	0.1207

ruthenate nanosheet features high two-dimensional crystallinity undoubtedly inherited from the parent material.

4. Conclusions

We have demonstrated that a layered protonic ruthenate mono-hydrate derived from layered potassium ruthenate, $H_{0.2}RuO_{2.1}\cdot 0.9H_2O$, can directly react with bulky tetrabutylammonium ions (TBA^+) to trigger total exfoliation into elemental single host layers of ruthenium oxide. Refinement of the reaction conditions allowed us to obtain exfoliated ruthenate nanosheets in high yield, 70%. Partially or completely dehydrated protonic ruthenates ($H_{0.2}RuO_{2.1}\cdot nH_2O$, $n = 0$, 0.5) have a low reactivity towards intercalation of the bulky exfoliation reagent. The presence of sufficient interlayer water is a key factor for the direct reaction as the expanded interlayer is essential for the incorporation of bulky species. The intercalation, swelling and exfoliation processes of the layered ruthenate are governed by the ratio of tetrabutylammonium ions to ion-exchangeable protons, similar to other layered oxide systems. The one-step process utilized in this work afforded high purity ruthenate nanosheets in a high yield, which permitted detailed characterization of the nanosheet. The ruthenate nanosheets were identified as a unilamellar two-dimensional crystallite of oblique symmetry. This study provided fundamental information on the formation and structural features of the ruthenate nanosheet, which will be useful for understanding its intriguing physicochemical properties and further studies directed toward many applications.

Acknowledgments

This work was supported in part by a "Creation of Innovation Centers for Advanced Interdisciplinary Research Areas" Project in Special Coordination Funds for Promoting Science and Technology of the Ministry of Education, Culture, Sports, Science and Technology, Japan and CREST of the Japan Science and Technology Agency (JST). The authors wish to thank Professor Takayoshi Sasaki (National Institute for Materials Science and Tsukuba University) for his liberal cooperation in the in-plane XRD measurement with the approval of the Photon Factory Program Advisory Committee (2007G652).

Appendix A. Supplementary material

Supplementary data associated with this article can be found in the online version at 10.1016/j.jssc.2009.08.012.

References

[1] G.F. Walker, Nature 187 (1960) 312.
[2] P.H. Nadeau, M.J. Wilson, W.J. McHardy, J.M. Tait, Science 225 (1984) 923.
[3] M.M.J. Treacy, S.B. Rice, A.J. Jacobson, J.T. Lewandowski, Chem. Mater. 2 (1990) 279.
[4] G. Alberti, M. Casciola, U. Costantino, J. Colloid Interf. Sci. 107 (1985) 256.
[5] A. Leaf, R. Schöllhorn, Inorg. Chem. 16 (1977) 2950.
[6] T. Sasaki, M. Watanabe, H. Hashizume, H. Yamada, H. Nakazawa, J. Am. Chem. Soc. 118 (1996) 8329.
[7] Z.-H. Liu, K. Ooi, H. Kanoh, W.-P. Tang, T. Tomida, Langmuir 16 (2000) 4154.
[8] R.E. Schaak, T.E. Mallouk, Chem. Commun. (2002) 706.
[9] S. Ida, C. Ogata, U. Unal, K. Izawa, T. Inoue, O. Altuntasoglu, Y. Matsumoto, J. Am. Chem. Soc. 129 (2007) 8956.
[10] M. Adachi-Pagano, C. Forano, J.-B. Besse, Chem. Commun. (2000) 91.
[11] T. Hibino, W. Jones, J. Mater. Chem. 11 (2001) 1321.
[12] N. Sakai, Y. Ebina, K. Takada, T. Sasaki, J. Phys. Chem. B 109 (2005) 9651.
[13] M. Osada, Y. Ebina, K. Takada, T. Sasaki, Adv. Mater. 18 (2006) 295.
[14] K. Fukuda, K. Akatsuka, Y. Ebina, R. Ma, K. Takada, I. Nakai, T. Sasaki, ACS Nano 2 (2008) 1689.
[15] D.M. Kaschak, J.T. Lean, C.C. Waraksa, G.B. Saupe, H. Usami, T.E. Mallouk, J. Am. Chem. Soc. 121 (1999) 3435.
[16] T. Sasaki, Y. Ebina, M. Watanabe, G. Decher, Chem. Commun. (2000) 2163.
[17] M. Muramatsu, K. Akatsuka, Y. Ebina, K. Wang, T. Sasaki, T. Ishida, K. Miyake, M. Haga, Langmuir 21 (2005) 6590.
[18] W.D. Ryden, A.W. Lawson, Phys. Rev. B 1 (1970) 1494.
[19] S. Trasatti, Electrochim. Acta 36 (1991) 225.
[20] S. Trasatti, in: S. Trasatti (Ed.), Electrodes of Conducting Metal Oxides, Elsevier, Amsterdam, Netherland, 1980, p. 301.
[21] W. Sugimoto, H. Iwata, Y. Yasunaga, Y. Murakami, Y. Takasu, Angew. Chem. Int. Ed. 42 (2003) 4092.
[22] W. Sugimoto, K. Yokoshima, K. Ohuchi, Y. Murakami, Y. Takasu, J. Electrochem. Soc. 153 (2006) 255.

[23] W. Sugimoto, T. Saida, Y. Takasu, Electrochem. Commun. 8 (2006) 411.
[24] D.M. Moore, J. Hower, Clays Clay Miner. 34 (1986) 379.
[25] Q. Gao, O. Giraldo, W. Tong, S.L. Suib, Chem. Mater. 13 (2001) 778.
[26] Y. Omomo, T. Sasaki, L.Z. Wang, M. Watanabe, J. Am. Chem. Soc. 125 (2003) 3568.
[27] T. Sasaki, M. Watanabe, J. Am. Chem. Soc. 120 (1998) 4682.
[28] T. Sasaki, Y. Ebina, Y. Kitami, M. Watanabe, T. Oikawa, J. Phys. Chem. B 105 (2001) 6116.
[29] K. Fukuda, I. Nakai, C. Oishi, M. Nomura, M. Harada, Y. Ebina, T. Sasaki, J. Phys. Chem. B 108 (2004) 13088.
[30] K. Fukuda, I. Nakai, Y. Ebina, M. Tanaka, T. Mori, T. Sasaki, J. Phys. Chem. B 110 (2006) 17070.